Direction de la recherche technologique
Département des technologies pour les énergies nouvelles
Service de Conversion et Stockage de l'énergie
Laboratoire Hydrogène et Pile à Combustible

**Rapport technique DTEN/DR/2003/167**

# *MODELLING AND SIMULATION OF THE FILLING OF A GASEOUS HYDROGEN TANK UNDER VERY HIGH PRESSURE*

# *[MODELISATION ET SIMULATION DU REMPLISSAGE D'UN RESERVOIR D'HYDROGENE GAZEUX SOUS TRES HAUTE PRESSION]*

*Christian PERRET*

| | |
|---|---|
| **Référence du contrat** | 769175 |
| **Référence PRODEM** | EIHP2 – 00-00111 |
| **Nature du rapport** | Final |
| **Confidentialité** | Les informations contenues dans le présent document sont la propriété des contractants. Il ne peut être reproduit ou transmis à des tiers sans l'autorisation expresse des contractants. |

| | **Rédacteur** | **Vérificateurs** | | **Approbateur** |
|---|---|---|---|---|
| **Nom** | Christian PERRET | S. CHAUDOURNE | P. SERRE-COMBE | D. SARTI |
| **Fonction** | Ingénieur de Recherche | Responsable Technique Hydrogène | Chef du LHPAC | Chef du SCSE |
| **Signature** | p.o. | | | P.O. |
| **Date** | 04/02/2004 | 04/02/2004 | 26/4/04 | 6.04.03 |

P. SERRE-COMBE

Direction de la recherche technologique
Département des technologies pour les énergies nouvelles
Service de Conversion et Stockage de l'énergie
Laboratoire Hydrogène et Pile à Combustible

Project EIHP2
Contract n° ENK6-CT2000-0042
WP 3.2

Technical Report

# Modelling and simulation of the filling of a gaseous hydrogen tank under very high pressure

Christian PERRET

January 2004

## LISTE DE DIFFUSION

Rapport complet à :

| | | |
|---|---|---|
| CLIENT : Union Européenne | R. WURSTER (LBST), | 1 ex. |
| | F. ISORNA (INTA) | 1 ex. |
| LITEN/FAR | P. LUCCHESE | 1 ex. |
| DTEN/DIR | J. DANROC | 1 ex. |
| DTEN/SCSE | D. SARTI | 1 ex. |
| SCSE/LHPAC | P. SERRE-COMBE | 1 ex. |
| | C. PERRET | 1 ex. |
| | S. CHAUDOURNE | 2 ex. |
| | Archivage | Original + 1 ex. |

Page de garde + résumé + Liste de diffusion à :

| | |
|---|---|
| DTEN/SMP | F. LE NAOUR |
| DTEN/SAT | F. TARDIF |
| DTEN/SCSE/GENEC | P. MALBRANCHE |
| DTEN/SCSE/LSEM | D. MARSACQ |
| DTEN/SCSE/GRETH | C. MARVILLET |

Page de garde + résumé + Liste de diffusion + Lettre d'envoi à :

| | |
|---|---|
| DTEN/QUALITE | J-F. NOWAK |
| DTEN/BF | S. VERMET |

## Résumé

**Français**
Ce rapport expose la méthodologie utilisée pour simuler le remplissage sous haute pression d'un réservoir d'hydrogène embarqué sur véhicule.

La technique des bond graphs est mise en oeuvre pour la décomposition du système en éléments thermo-hydrauliques simples dont les équations sont énoncées.

Les propriétés du gaz réel sont prises en compte pour restituer le comportement de l'hydrogène aux hautes pressions.

Une comparaison entre calcul et résultats expérimentaux est présentée.
Les influences de la durée du remplissage et des propriétés thermiques de la paroi du réservoir sur les températures sont étudiées.

**English**
This report presents the methodology used to simulate on board tank filling under high pressure.

The system is split according to Bond graphs technique in simple thermohydraulic elements. Governing equations are given.

Real gas properties are taken in account for hydrogen behaviour under high pressure.

Comparison between computational and experimental results is presented.
Influences of filling duration and tank wall thermal properties on temperatures are studied.

## Mots clés

Hydrogène, haute pression, réservoir, remplissage, modélisation, bond graphs, gaz réel.

# INTRODUCTION

This work has been realised in the frame of the European project EIHP2.

The objective of the work package 3.2 of this project is the definition of CGH2 refuelling procedure.

The fast filling of vehicle tank at a hydrogen service station must be carefully studied because severe thermal problems can occur during the operation : freezing of the flexible and connector due to gas pressure drop in the flow and high temperature rise of the vessel internal wall due to fast pressure rise inside the vessel.

For a better understanding of these physical phenomena, CEA developed experimental and simulation approaches.

At CEA – Valduc an experimental device was realised to test Hydrogen transfer under 350 bars pressure.
At first, the permeability to hydrogen of a GPL connector (Staübli) was measured. Then, the filling of a composite vessel with polymer liner was experimented. Pressure and temperature evolution were registered during filling and cooling of the receiver tank at various points of the circuit.

At CEA – Grenoble, modelling tools for Hydrogen transfer simulation were developed.
A modular set of 0-D thermal and hydraulic elements has been realised for a bond graph modelling of a gas circuit. At high pressure, ideal gas model is not valid, so real gas properties were taken in account.
The experimental device was then simulated.

This document presents this simulation work and comparison between computational and experimental results.

# I. Experiment description

The test was performed in two stages, illustrated on Figure 1 :

- A. Test of connector.

Five 10 l tanks under a 350 bar pressure are used for feeding. The connector is in a closed chamber equipped with a leakage detector. Hydrogen is released in the atmosphere. Pressure evolution in the feeding tanks is recorded.

- B. Filling test of the 9 litres composite tank.

A 9 l tank with polyamide liner and composite structure is connected. Pressure evolution is recorded in the feeding tanks. Internal gas temperature and external wall temperature are measured in the receptor tank.

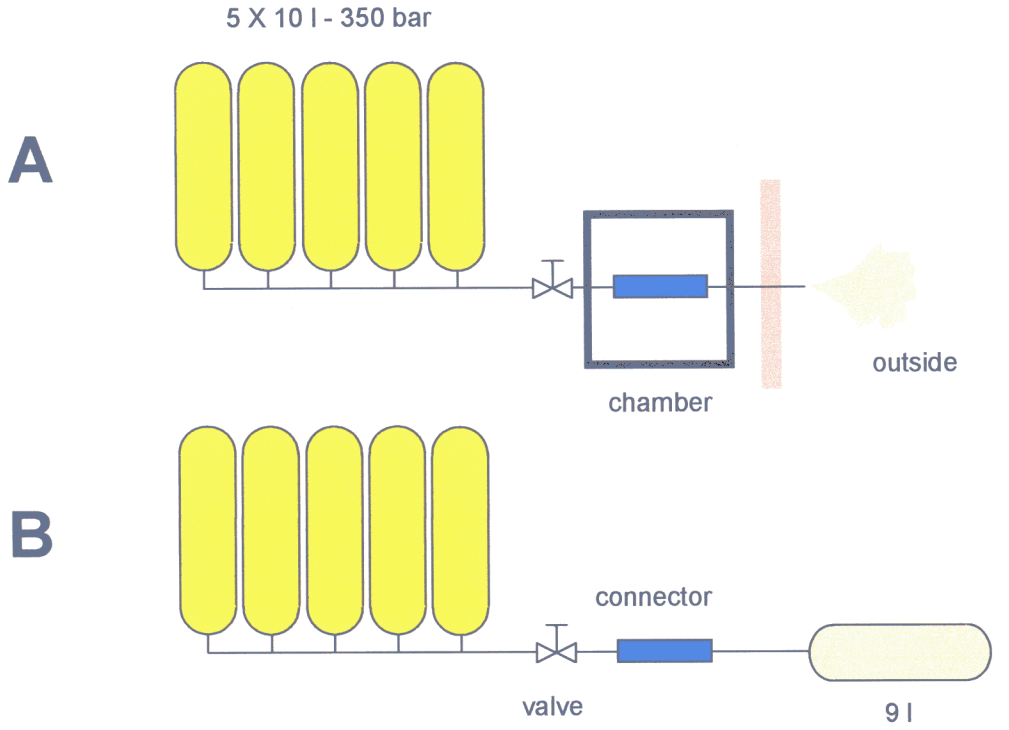


Figure 1 : experimental device

It is important to mention that piping diameter has been chosen in the aim to limit the flow rate only by the connector which has the smallest cross flow section of the circuit.

In this work, only the hydraulic and thermal aspects of gas transfer are studied. We do not consider connector sealing problem.

# II. Modelling

### *II.1 Real gas model*

We focused on the hydraulic and thermal aspects of gas transfer under high pressure. So a special care has been done to the hydrogen properties under high pressure. It is obvious that perfect gas model is not adapted in this case. The selected real gas equations models we have used are presented in this paragraph.

(These models are also used in the FLUENT CFD code for real gas modelling [1])

The following nomenclature applies to this section :

| | | |
|---|---|---|
| $a(T)$ | : | Redlich-Kwong temperature fonction |
| $c$ | : | speed of sound |
| $c_p$ | : | specific heat |
| $h$ | : | specific enthapy |
| $n$ | : | exponent in function $a(T)$ |
| $p$ | : | pressure |
| $r$ | : | hydrogen perfect gas constant $(r = R/M)$ |
| $T$ | : | temperature |
| $s$ | : | specific entropy |
| $\upsilon$ | : | specific volume |
| $\rho$ | : | density |
| $M$ | : | molar mass |

### II.1.1 *Specific volume and density*

The Redlich-Kwong equation of state is :

$$p = \frac{rT}{(\upsilon - \tilde{b})} - \frac{a(T)}{\upsilon(\upsilon + b_0)} \quad \text{(II.1-1)}$$

with

$$\upsilon = \frac{1}{\rho}, \qquad a(T) = \left(\frac{T}{T_c}\right)^n, \qquad a_0 = 0.42747\frac{r^2 T_c^2}{p_c},$$

$$b_0 = 0.08664\frac{rT_c}{p_c}, \qquad c_0 = \frac{rT_c}{p_c + \dfrac{a_0}{\upsilon_c(\upsilon_c + b_0)}} + b_0 - \upsilon_c, \qquad \tilde{b} = b_0 - c_0$$

The subscript $0$ designates a reference state, and the subscript $c$ designates a critical point property.

For convenience, equation (II.1-1) can be written as a cubic equation for specific volume as follows:

$$\upsilon^3 + a_1\upsilon^2 + a_2\upsilon + a_3 = 0 \quad \text{(II.1-2)}$$

with

$$a_1 = -\left(c + \frac{rT}{p}\right), \qquad a_2 = -\left(\tilde{b}\,b_0 + \frac{rTb_0}{p} - \frac{a(T)}{p}\right), \qquad a_3 = -\frac{a(T)\tilde{b}}{p}$$

Equation (II.1-2) is solved using a standard algorithm minimizing the number of floating points operation for optimal performance.

### II.1.2 Specific heat and enthalpy

Enthalpy for a real gas can be written:

$$h = h^0(T) + p\upsilon - rT - \frac{a(T)}{b_0}(1+n)\ln\left(\frac{\upsilon + b_0}{\upsilon}\right) \quad (\text{II.1-3})$$

where $h^0(T)$ is the enthalpy function for a thermally perfect gas (i.e., enthalpy is a function of temperature alone). In the present case, we employ a fourth-order polynomial for the specific heat for a thermally perfect gas:

$$c_p^0(T) = C_1 + C_2T + C_3T^2 + C_4T^3 + C_5T^4 \quad (\text{II.1-4})$$

and obtain the enthalpy from the basic relation:

$$h^0(T) = \int_{T_0}^{T} c_p^0(T)\,dT \quad (\text{II.1-5})$$

The result is:

$$h^0(T) = C_1T + \frac{1}{2}C_2T^2 + \frac{1}{3}C_3T^3 + \frac{1}{4}C_4T^4 + \frac{1}{5}C_5T^5 - h^0(T^0) \quad (\text{II.1-6})$$

Note that $h^0(T^0)$ is the enthalpy at a state reference $(p^0, T^0)$, which can be chosen arbitrarily. The specific heat for the real gas can be obtained by differentiating equation ( II.1-3) with respect to temperature:

$$c_p = \left(\frac{\partial h}{\partial T}\right)_p \quad (\text{II.1-7})$$

The result is:

$$c_p = c_p^0(T) + p\upsilon\left(\frac{\partial \upsilon}{\partial T}\right)_p - r - \frac{da(T)}{dT}\frac{(1+n)}{b_0}\ln\left(\frac{\upsilon + b_0}{\upsilon}\right) + a(T)(1+n)\frac{\left(\frac{\partial \upsilon}{\partial T}\right)_p}{\upsilon(\upsilon + b_0)} \quad (\text{II.1-8})$$

### II.1.3 Entropy

The entropy can be expressed in the form:

$$s = s^0(T, p^0) + r\ln\left(\frac{\upsilon - \tilde{b}}{\upsilon^0}\right) + \frac{\left(\frac{da(T)}{dT}\right)}{b_0}\ln\left(\frac{\upsilon + b_0}{\upsilon}\right) \quad (\text{II.1-9})$$

where the subscript 0 again refers to a reference state where the perfect gas law is applicable. For an ideal gas at fixed reference pressure, $p^0$ ,the entropy is given by:

$$s^0(T,p^0) = s^0(T^0,p^0) + \int_{T^0}^{T} \frac{c_p^0(T)}{T} dT \quad \text{( II.1-10)}$$

Using the polynomial expression for specific heat, ( II.1-10) becomes:

$$s^0(T,p^0) = s^0(T^0,p^0) + C_1 \ln(T) + C_2 T \frac{1}{2} C_3 T^2 + \frac{1}{3} C_4 T^3 + \frac{1}{4} C_5 T^4 - f(T^0) \quad \text{(II.1-11)}$$

where $f(T^0)$ is constant, which can be absorbed into the reference entropy $s(T^0,p^0)$.

### *II.1.4 Speed of sound*

The speed of sound for a real gas can be determined from the thermodynamic relation:

$$c^2 = \left(\frac{\partial p}{\partial \rho}\right)_p = -\left(\frac{c_p}{c_v}\right)\frac{\upsilon^2}{\left(\frac{\partial \upsilon}{\partial p}\right)_T} \quad \text{(II.1-12)}$$

### *II.1.5 Viscosity and thermal Conductivity*

The dynamic viscosity of a gas or vapour can be estimated by using the following formula :

$$\mu(T) = 6.3\times10^7 \frac{M^{0.5} P_c^{0.6666}}{T_c^{0.1666}} \left(\frac{T_r^{1.5}}{T_r + 0.8}\right) \quad \text{(II.1-13)}$$

Here, $T_r$ is the reduced temperature:

$$T_r = \frac{T}{T_c} \quad \text{(II.1-14)}$$

And $M$ is the molar mass of the gas.

Knowing the viscosity, the thermal conductivity can estimated by using the Eukum formula:

$$k = \mu\left(c_p + \frac{5}{4} r\right) \quad \text{(II.1-15)}$$

### *II.1.6 Parameters values for hydrogen*

$r = 8314.34/M \quad (\text{J/kg.K})$

$M = 2.0159 \quad (\text{kg/kmol})$

$P_c = 1.2838\cdot10^6 \quad (\text{Pa})$

$T_c = 32.938 \quad (\mathrm{K})$

$V_c = 3.188788 \cdot 10^{-2} \quad (\mathrm{m^3/kg})$

$n = \quad 0.310$

$C_1 = 12594.6,\ C_2 = 11.02903,\ C_3 = -2.134119 \cdot 10^{-2},\ C_4 = 2.274608 \cdot 10^{-5},$

$C_5 = -7.465296 \cdot 10^{-9}$

$p_{ref} = 101325 \quad (\mathrm{Pa})$

$T_{ref} = 288.15 \quad (\mathrm{K})$

## *II.2 System modelling*

### *II.2.1 Global scheme*

We use a bond graph approach for modelling [2]. The main principles of this method, frequently used in industry for system modelling can be briefly exposed:

- All kind of systems (mechanical, thermal, hydraulic, chemical...) are analysed using analogy to electrical circuit.
- Elements of the system and links between them are presented graphically. Elementary elements of the graph are generally 0-D models.
- The resulting bond graph includes "causality analysis" to formulate a numerical system easy to solve.

Dedicated software allow to work directly with bond graph formalism. We used "20Sim" in this study. It appeared to be a very efficient and versatile tool for system modelling.

#### II.2.1.1 Experiment "A" bond graph

The bond graph of the first stage "A" of the experiment is presented above:


Figure 2 : Experiment "A" bond graph.

In this scheme:

- The gas capacity Tank_1 represents the five feedings tanks. No thermal exchange through wall (adiabatic).
- Piping and connector are modelled as a hydraulic resistance.
- Atmospheric pressure is imposed as an effort source (boundary condition).

### II.2.1.2 Experiment "B" bond graph

The receptor tank is now represented with wall (Tank_2 on Figure 3):

- The liner and the composite structure are modelled separately with two thermal capacities.
- Convective thermal transfer in the tank (H2-wall) and outside (wall-air) are figured by thermal resistance.
- Thermal contact resistance between liner and structure is taken in account:

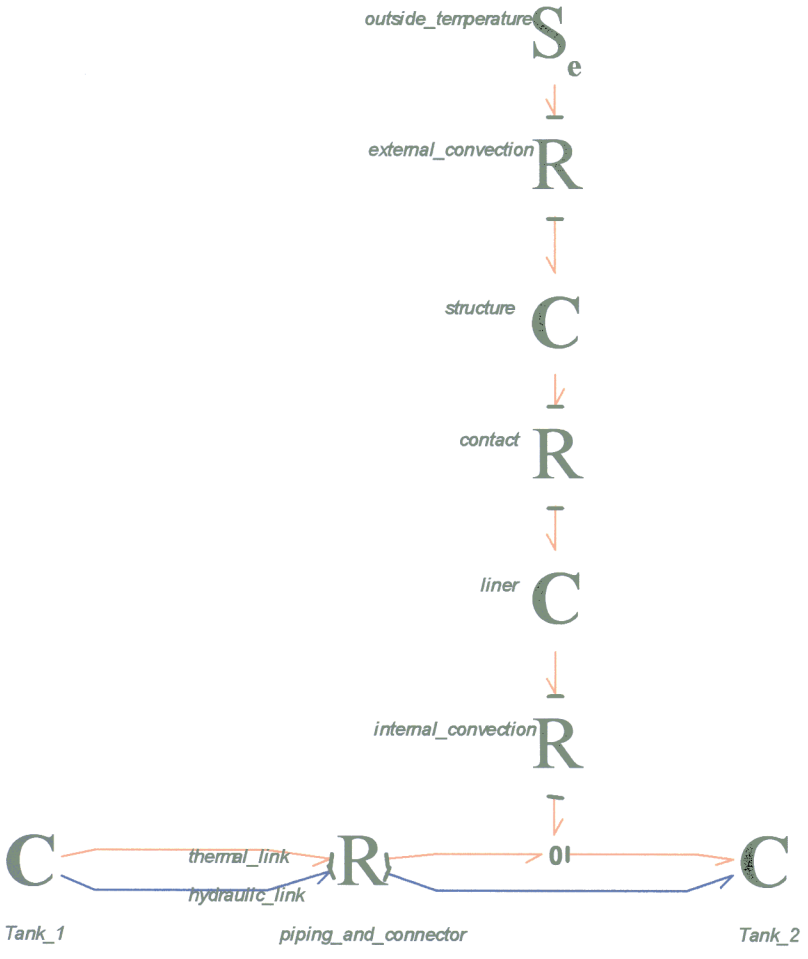


Figure 3 : Experiment "B" bond graph.

### *II.2.2 Tanks modelling*

Mass and internal energy balance in Tank_1 are:

$$M_1 = \int_0^t -\dot{M}_{1\to 2}\, dt + M_1^0 \qquad \text{(II.2-1)}$$

$$U_1 = \int_0^t -\dot{H}_{1\to 2}\, dt + U_1^0 \qquad \text{(II.2-2)}$$

With :

$M_1$ : Tank_1 total gas mass,

$U_1$ : Tank_1 total internal energy,

$\dot{M}_{1\to 2}$ : mass flow rate from Tank_1 to Tank2,

$\dot{H}_{1\to 2}$ : enthalpy flow rate from Tank_1 to Tank2.

$(p_1, T_1)$ are solutions of :

$$\rho(p_1, T_1) = \frac{M_1}{V_1} \quad \text{(II.2-3)}$$

$$u(p_1, T_1) = \frac{U_1}{M_1} \quad \text{(II.2-4)}$$

Mass and internal energy balance in Tank_2 are:

$$M_2 = \int_0^t \dot{M}_{1\to 2}\, dt + M_2^0 \quad \text{(II.2-5)}$$

$$U_2 = \int_0^t \left(\dot{H}_{1\to 2} + \dot{Q}_{L\to 2}\right) dt + U_2^0 \quad \text{(II.2-6)}$$

With :

$M_2$ : Tank_2 total gas mass,

$U_2$ : Tank_2 total internal energy,

$\dot{Q}_{L\to 2}$ : heat flux from liner to gas.

$(p_2, T_2)$ are solutions of :

$$\rho(p_2, T_2) = \frac{M_2}{V_2} \quad \text{(II.2-7)}$$

$$u(p_2, T_2) = \frac{U_2}{M_2} \quad \text{(II.2-8)}$$

### *II.2.3 Connector and piping modelling*

The piping and the connector between the two tanks constitute a nozzle [3]. At inlet, the conditions are given by Tank_1:

$$\begin{aligned} p &= p_1 \\ T &= T_1 \\ v &= 0 \end{aligned} \quad \text{(II.2-9)}$$

We can assume that the flow is adiabatic and non-viscous. In these conditions, entropy and energy are constant along the nozzle and $(p,T,v)$ verify:

$$s(p,T) = s(p_1,T_1) = C^{ste} \quad \text{(II.2-10)}$$

$$h(p,T) + \frac{1}{2}v^2 = h(p_1,T_1) = C^{ste} \quad \text{(II.2-11)}$$

At first, critical conditions $(p_c,T_c,v_c)$ (reached when flow velocity is equal to sound velocity) are to be computed, by solving the following equations:

$$s(p_c,T_c) = s(p_1,T_1) \quad \text{(II.2-12)}$$

$$h(p_c,T_c) + \frac{1}{2}v_c^2 = h(p_1,T_1) \quad \text{(II.2-13)}$$

$$v_c = c(p_c,T_c) \quad \text{(II.2-14)}$$

If $p_2 \le p_c$, the nozzle flow rate is critical:

$$\dot{M}_{1\to 2} = \beta_c \, S_c \, \rho(p_c,T_c) \, v_c \quad \text{(II.2-15)}$$

With :

$0 < \beta \le 1$: constriction coefficient,

$S_c$: connector section.

Else if $p_2 > p_c$, outlet nozzle conditions $(p_2,\tilde{T}_2,v_2)$, are given by :

$$s(p_2,\tilde{T}_2) = s(p_1,T_1) \quad \text{(II.2-16)}$$

$$h(p_2,\tilde{T}_2) + \frac{1}{2}v_2^2 = h(p_1,T_1) \quad \text{(II.2-17)}$$

And then :

$$\dot{M}_{1\to 2} = \beta_c \, S_c \, \rho(p_2,\tilde{T}_2) \, v_2 \quad \text{(II.2-18)}$$

**Remark:** generally $T_2 \neq \tilde{T}_2$

The enthalpy flow rate is calculated with an upwind scheme:

$$\dot{H}_{1\to 2} = \dot{M}_{1\to 2} \, h(p_1,T_1) \quad \text{(II.2-19)}$$

### II.2.4 *Tank_2 wall modelling*

The thermal transient equation is solve in the liner and in the structure. Three heat transfer coefficients have to be estimated:

- A convective heat transfer coefficient $\alpha_{conv}$ in the tank,
- A contact heat transfer coefficient $\alpha_{contact}$ between the liner and the composite structure,
- An external convective heat transfer $\alpha_{ext}$.

Figure 4 summarize Tank_2 wall modelling:

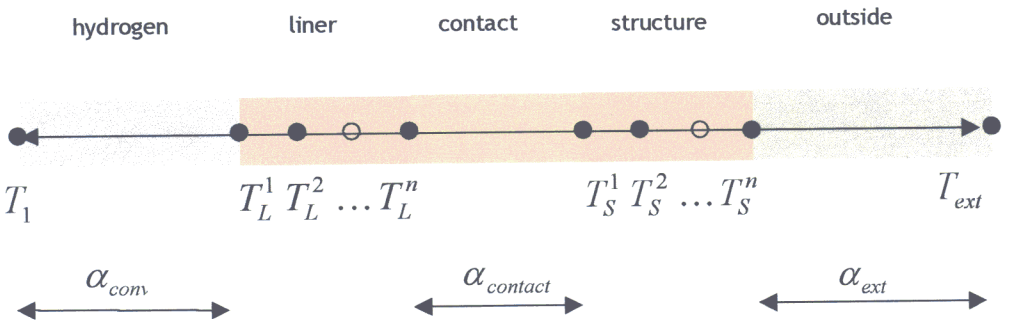


Figure 4

#### II.2.4.1 Conduction in the liner

The liner is meshed with n temperature nodes. Thermal diffusion equations in the liner are:

$$[H]_L = \int_0^t [\varphi]_L dt + [H^0]_L \quad \text{(II.2-20)}$$

$$[\varphi]_L = [C]_L [T]_L + [\varphi]_L^{ext} \quad \text{(II.2-21)}$$

With :

$$[T]_L = \begin{vmatrix} T_L^1 \\ T_L^i \\ T_L^n \end{vmatrix}, \qquad [C]_L = \frac{\lambda_L (n-1) S_2}{e_L} \begin{vmatrix} -1 & 1 & & & 0 \\ 1 & -2 & & & \\ & . & . & . & \\ & & 1 & -2 & 1 \\ 0 & & & 1 & -1 \end{vmatrix}, \qquad [\varphi]_L^{ext} = \begin{vmatrix} -\dot{Q}_{L\to 2} \\ 0 \\ \dot{Q}_{S\to L} \end{vmatrix}$$

$\dot{Q}_{L\to 2}$ heat flux from liner to gas,

$\dot{Q}_{S\to L}$ heat flux from structure to liner,

$\lambda_L$ liner thermal conductivity,

$n$ number of temperature nodes,

$S_2$ Tank_2 mean surface,

$e_L$ liner thickness.

Temperatures $[T]_L$ are computed from:

$$[I]_L[T]_L = [H]_L \quad \text{(II.2-22)}$$

With :

$$[I]_L = \frac{c_{p_L}\, e_L\, S_2}{(n-1)} \begin{vmatrix} 1/2 & 0 & & & 0 \\ 0 & 1 & 0 & & \\ & . & . & . & \\ & & 0 & 1 & 0 \\ 0 & & & 0 & 1/2 \end{vmatrix}$$

$c_{p_L}$ : liner specific heat.

### II.2.4.2 Heat conduction in the structure

The structure is meshed with n temperature nodes. Thermal diffusion equation in the structure are:

$$[H]_S = \int_0^t [\varphi]_S dt + [H^0]_S \quad \text{(II.2-23)}$$

$$[\varphi]_S = [C]_S[T]_S + [\varphi]_S^{ext} \quad \text{(II.2-24)}$$

Where:

$$[T]_S = \begin{vmatrix} T_S^1 \\ T_S^i \\ T_S^n \end{vmatrix}, \qquad [C]_S = \frac{\lambda_S (n-1) S_2}{e_S} \begin{vmatrix} -1 & 1 & & & 0 \\ 1 & -2 & & & \\ & . & . & . & \\ & & 1 & -2 & 1 \\ 0 & & & 1 & -1 \end{vmatrix}, \qquad [\varphi]_S^{ext} = \begin{vmatrix} -\dot{Q}_{S\to L} \\ 0 \\ \dot{Q}_{ext} \end{vmatrix}$$

$\dot{Q}_{ext}$ heat flux from air to structure

$\dot{Q}_{S\to L}$ heat flux from structure to liner

$\lambda_S$ structure thermal conductivity

$n$ number of temperature nodes

$e_S$ structure thickness

$S_2$ mean surface

Temperatures $[T]_S$ are computed by:

$$[I]_S[T]_S = [H]_S \quad \text{(II.2-25)}$$

With :

$$[I]_S = \frac{c_{pS}\ e_S\ S_2}{(n-1)} \begin{vmatrix} 1/2 & 0 & & & 0 \\ 0 & 1 & 0 & & \\ & . & . & . & \\ & & 0 & 1 & 0 \\ 0 & & & 0 & 1/2 \end{vmatrix}$$

$c_{pS}$ specific heat.

### II.2.4.3 Heat transfer between liner and structure

$$\dot{Q}_{S\to L} = \alpha_{contact} S_2 \left(T_S^1 - T_L^n\right) \quad \text{(II.2-26)}$$

In our model $\alpha_{contact} = C^{ste}$

### II.2.4.4 External heat transfer

$$\dot{Q}_{ext} = \alpha_{ext} S_2 \left(T_{ext} - T_S^n\right) \quad \text{(II.2-27)}$$

In our model $\alpha_{ext} = C^{ste}$.

### II.2.4.5 Convective heat transfer between liner and gas

$$\dot{Q}_{L\to 2} = \alpha_{conv} S_2 \left(T_L^1 - T_2\right) \quad \text{(II.2-28)}$$

Grashof, Prandtl and Reynolds numbers are:

$$Gr = \frac{g\,\rho^2\,\beta\,\theta\,L^3}{\mu^2},$$

$$Pr = \frac{\mu\,c_p}{\lambda},$$

$$Re = \frac{\rho\,U\,L}{\mu}$$

Non dimensional numbers are computed with film properties at temperature :

$$T_f = \frac{T_L^1 + T_2}{2} \quad \text{(II.2-29)}$$

Length $L$ is equal to Tank_2 diameter: $L = D_2$

Reynolds number is computed from the average mass flux in the cross flow section of Tank_2:

$$\mathrm{Re} = \left( \frac{4\dot{M}_{1\to 2}}{\pi D_2^2} \right) \frac{D_2}{\mu} \quad \text{(II.2-30)}$$

Figure 5 shows non dimensional numbers values during the simulation. Two stages have two be considered:

1. filling with forced convection,
2. cooling with free convection.

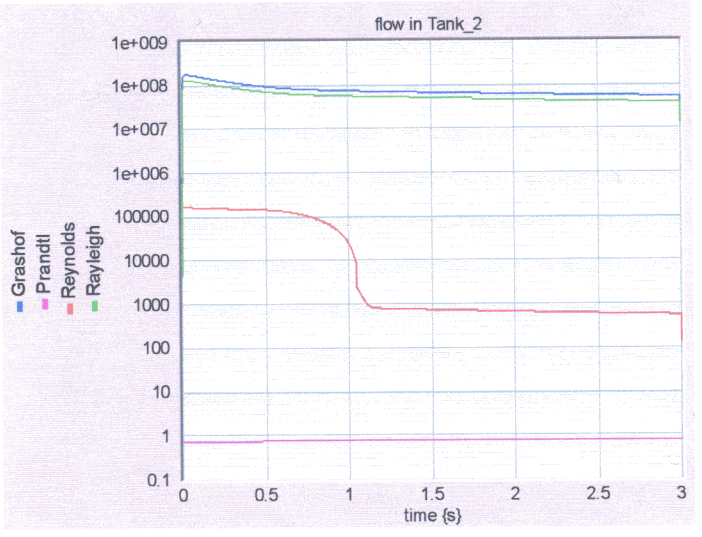


Figure 5

The heat exchange coefficient is deduced from the Nusselt number:

$$\alpha_{conv} = Nu \frac{\lambda}{D_2} \quad \text{(II.2-31)}$$

The forced convection Nusselt number is taken from the Bibliography:

$$Nu = 0.0366 \mathrm{Pr}^{1/3} \mathrm{Re}^{4/5} \quad \text{(II.2-32)}$$

The Formulation of free convection Nusselt is:

$$Nu = A(Gr.Pr)^m \quad \text{(II.2-33)}$$

In this case, the coefficient values provided by bibliography do not give satisfying results, so we adjust them to get a good fitting between computation and experiment:

$$A = 2.0,\ m = 0.287$$

Figure 6 shows values of heat exchange coefficient at the beginning of the simulation. The resulting coefficient is :

$$\alpha_{conv} = \max\left\{\alpha_{forced\_conv}, \alpha_{free\_conv}\right\} \quad \text{(II.2-34)}$$

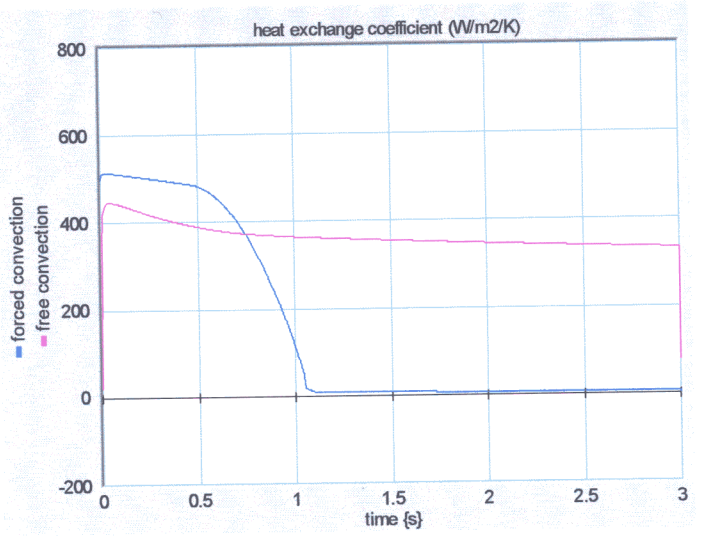


Figure 6

# III. Simulation results

## *III.1 Data*

Tank_1:

$$V_1 = 0.050\ \mathrm{m}^3$$

Tank_2:

$$V_2 = 0.009\ \mathrm{m}^3, S_2 = 0.25\ \mathrm{m}^2, D_2 = 0.16\ \mathrm{m}$$

Liner (Polyamide 6)

$$e_L = 0.002\ \mathrm{m},\ c_{pL} = 1250\ \mathrm{J \cdot Kg^{-1}\ K^{-1}}, \lambda_L = 0.25\ \mathrm{W \cdot m^{-1} K^{-1}}, \rho_L = 1100.\ \mathrm{Kg \cdot m^{-3}}$$

Structure (60% carbon + 40% epoxy):

$$e_S = 0.008\ \mathrm{m},$$

$$\lambda_S = 0.6 \times 175 + 0.4 \times 0.3 = 105.\ \mathrm{W \cdot m^{-1} K^{-1}}$$

$$\rho_S = 0.6 \times 1800 + 0.4 \times 1150 = 1540.\ \mathrm{Kg \cdot m^{-3}}$$

$$c_{ps} = (0.6 \times 1800 \times 800 + 0.4 \times 1150 \times 1200)/1540 = 1106.5\ \mathrm{J \cdot Kg^{-1}\ K^{-1}}$$

Connector:

$$S_c = 44.10^{-6}\ \mathrm{m}^2,\ D_c = 0.0075\ \mathrm{m}$$

Heat transfer coefficients :

$$\alpha_{ext} = 5.0\ \mathrm{W \cdot m^{-2}\ K^{-1}}$$

$$\alpha_{contact} = 100.0\ \mathrm{W \cdot m^{-2}\ K^{-1}}$$

### *III.2 Test A*

The results of this first experiment were only used to determine the constriction coefficient associated to the connector. Its value was adjusted to fit computed pressure in Tank_1 with experimental values. We obtained:

$$\beta_c = 0.18$$

| | Temperature (°C) | Time (s) | Tank_1 Pressure (bar) experiment | Tank_1 Pressure (bar) simulation |
|---|---|---|---|---|
| Test 2 | 16 | 0.00 | 307.43 | 307.43 |
| | | 9.80 | 50.40 | 52.74 |
| | | 28.75 | 12.22 | 5.8 |
| Test 3 | 16 | 0.00 | 329.08 | 329.08 |
| | | 11.00 | 50.80 | 46.66 |
| | | 26.00 | 9.86 | 8.01 |
| Test 6 | 23 | 0.00 | 401.33 | 401.33 |
| | | 12.00 | 51.05 | 46.27 |
| | | 26.00 | 10.16 | 9.75 |

Table 1

The temperature mentioned in Table 1 is initial external temperature.

### *III.3 Test B*

Filling and cooling have to be separately analysed.

#### *III.3.1 Filling*

Figure 7 shows experimental and computed pressure evolutions in the tanks:

| pressures | experiment | computation |
|---|---|---|
| Tank_1 | X | X |
| tank_2 | (not available) | X |
| critical pressure in the connector | | X |

The filling time is very short ($\cong$ 1s).

We can see a good fitting between experimental and computational results with the previously determined constriction coefficient. The little gap on final pressure in Tank_1 (feeding tanks) can be explained by the fact that in the computation of the piping volume is not taken into account.

Figure 8 shows experimental and computed temperature evolution in Tank_2 (receiver) :

| Tank_2 temperatures | experiment | computation |
|---|---|---|
| Gas | X | X |
| wall external side temperature | X | X |

We can observe a delay in the thermal sensor response and computation certainly gives a more realistic temperature rise. However, computed maximum gas temperature is very close to the experimental value.

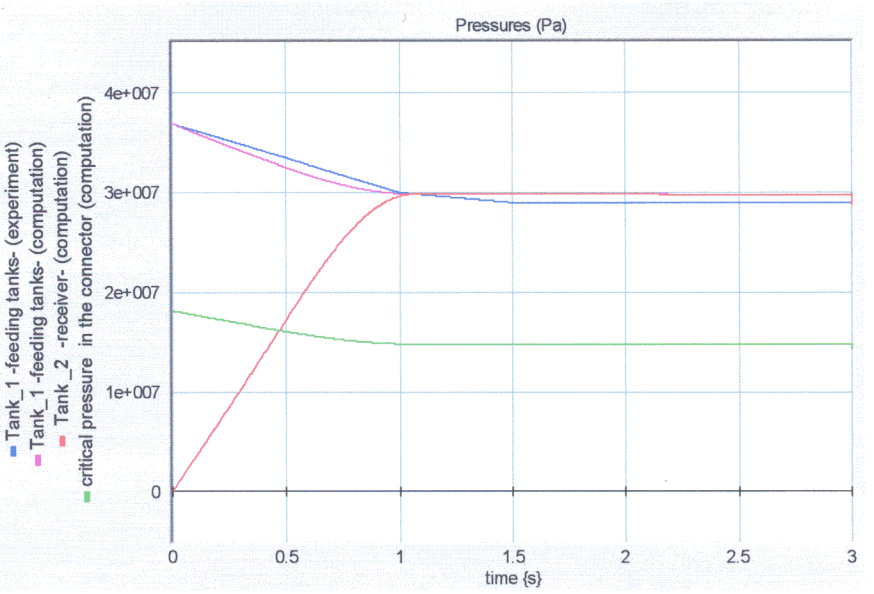


Figure 7

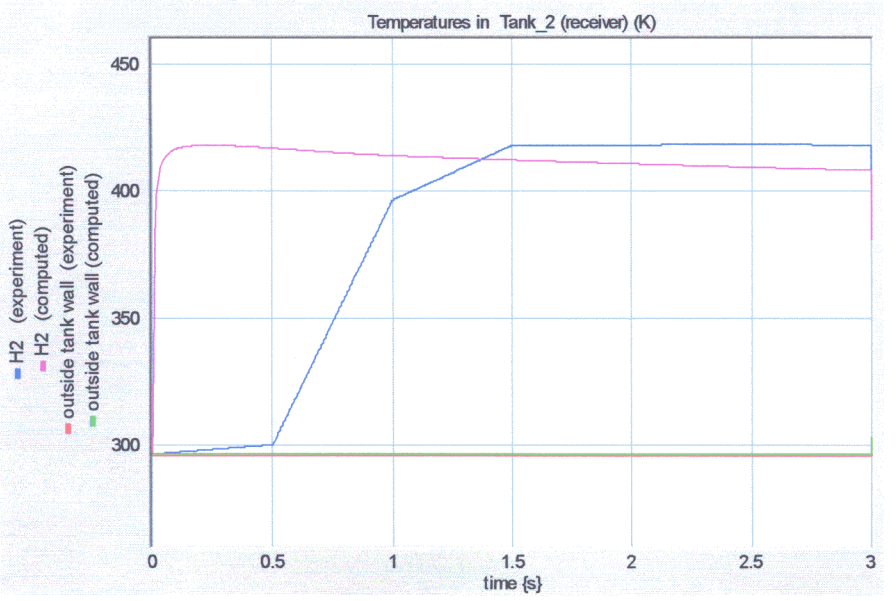


Figure 8

Figure 9 shows various computed temperatures and in particular the gas temperature in the connector.

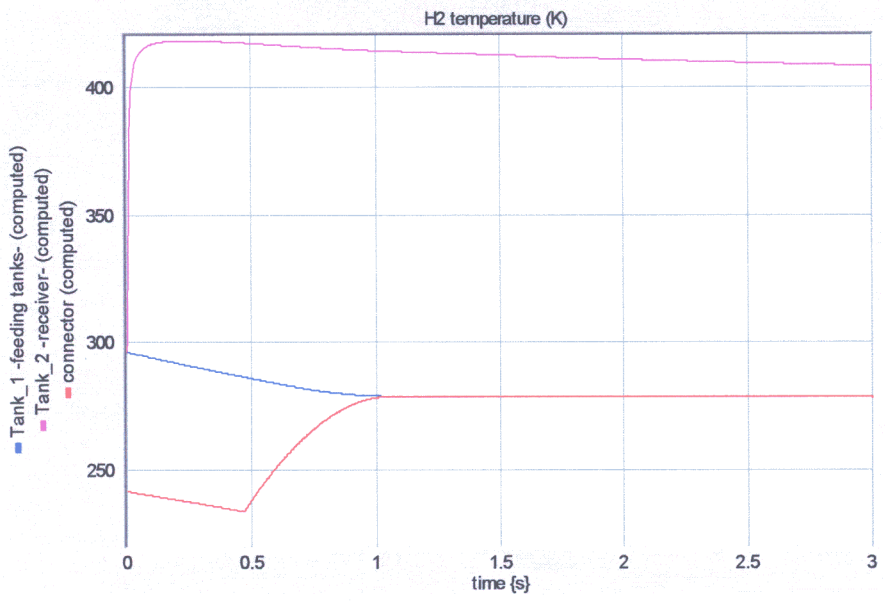


Figure 9

*III.3.2* *Cooling*

Figure 10 shows computed and experimental temperatures of Tank_2 wall :

| temperatures | experiment | computation |
|---|---|---|
| gas | X | X |
| wall external side | X | X |

(Notice that computed curves have been fitted by adjustment of the heat transfer coefficient)

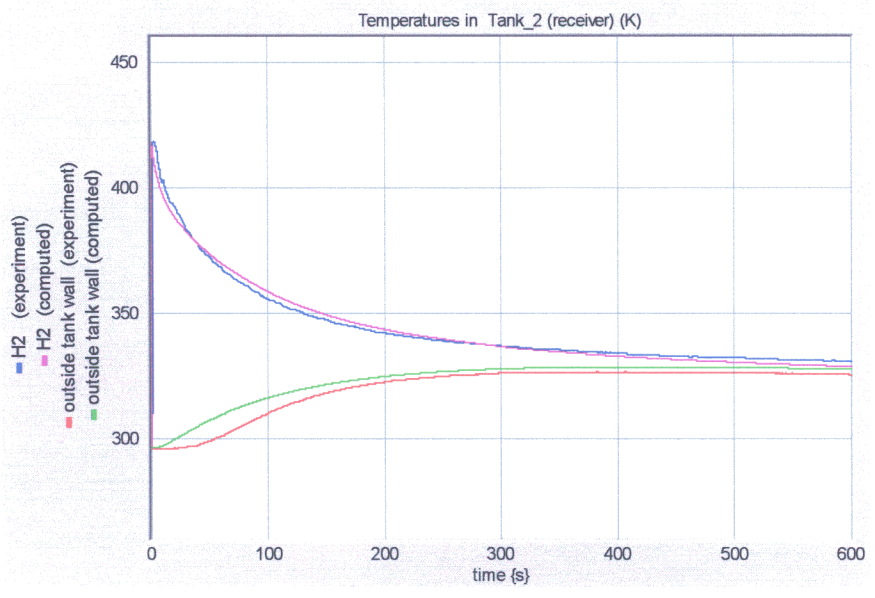


Figure 10

# IV. Parametric analysis

### *IV.1 Influence of filling duration on temperature*

Variations of the connector section have been used to vary the filling duration (they are inversely proportional). Figure 11 shows the mass evolution for various connector sections, Figure 12 and Figure 13 show corresponding gas temperature and liner surface temperature.

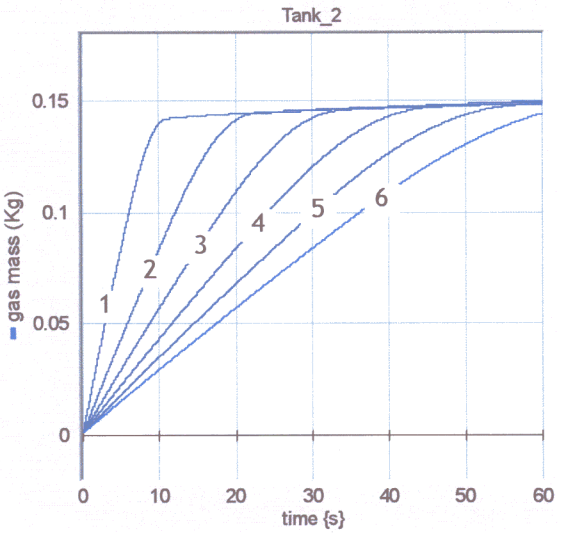


Figure 11

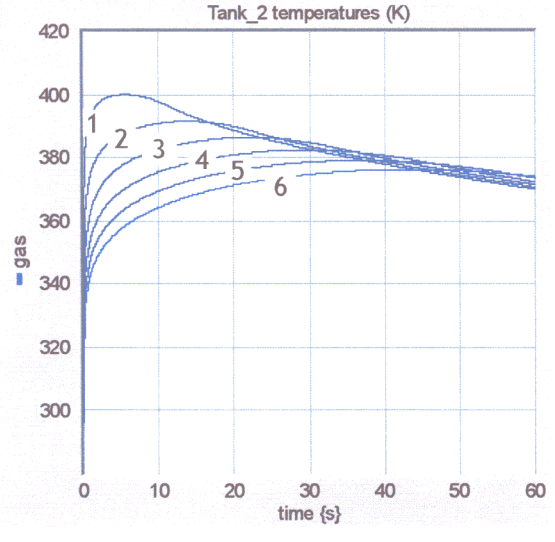


Figure 12

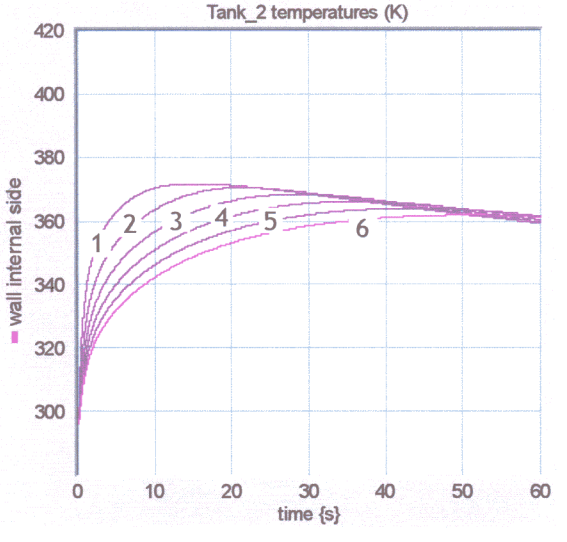


Figure 13

We can observe that temperature decreases significantly with filling duration augmentation.

### *IV.2 Influence of liner material on temperature (aluminium liner instead of polymer liner)*

We considered an aluminium liner, with the following properties :

$$e_L = 0.002\ \mathrm{m},\ c_{pL} = 900.\ \mathrm{J \cdot Kg^{-1}\ K^{-1}},\ \lambda_L = 22.\ \mathrm{W \cdot m^{-1} K^{-1}},\ \rho_L = 2700.\ \mathrm{Kg \cdot m^{-3}}$$

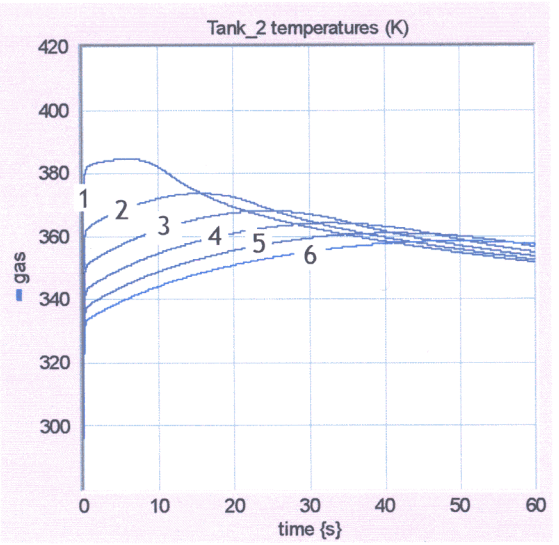


Figure 14

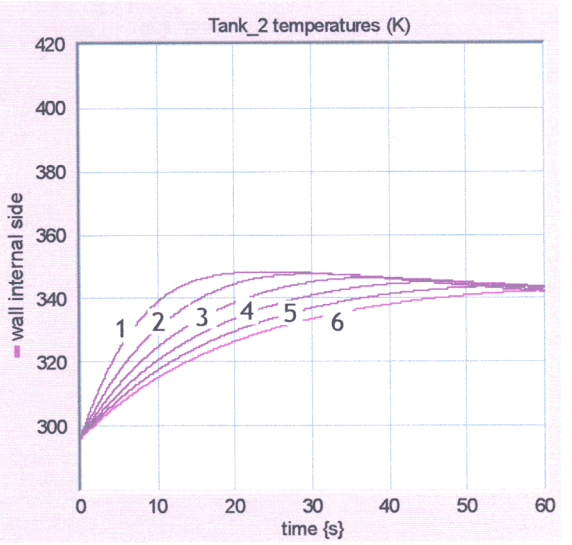


Figure 15

We can verify that, with an aluminium liner, temperatures are lower than with a polymer liner.

# CONCLUSION

The main result of this work is a better understanding of the thermal and hydraulic phenomena which occurs during the fast filling of a hydrogen tank under high pressure. The software developed would be a useful tool to obtain a better definition of the tank filling process and to help the tank design procedure.

It is important to notice that the experimental and modelling results presented here are not representative of real filling conditions. The experimental conditions (very small downwards tank and no hydrogen flow rate limitation) have been chosen to simplify the experimental procedure and minimize the costs. This explains the very high inside wall temperature obtained.

In fact the simulation performed with realistic parameter leads to acceptable inside wall temperatures if the hydrogen inlet temperature is sufficiently low (necessity in some cases to cool the hydrogen before filling).

Meanwhile we consider that the experimental data obtained to validate the model are not completely sufficient and we think that they would have to be completed to obtain a reliable simulation tool. In particular additional experimental data seemed to be necessary to validate the heat transfer coefficient between gas and tank wall during filling.

# BIBLIOGRAPHY

[1] FLUENT 6.1 Users' Guide, Fluent Inc., 2003S.

[2] G. Dauphin-Tanguy, Les bond graphs, HERMES Sciences Publications, 2000.

[3] Candel, Mécanique des fluides, Dunod, Paris, 2001.